Preprints of the 19th World Congress
The International Federation of Automatic Control
Cape Town, South Africa. August 24-29, 2014

Networked Embedded Control of Modular Robot Manipulators Using VDC

Wen-Hong Zhu * **Tom Lamarche** * **Erick Dupuis** *
Guangjun Liu **

* *Space Exploration, Canadian Space Agency*
6767 route de l'Aeroport, Saint-Hubert, QC, Canada J3Y 8Y9
(E-mails: *Wen-Hong.Zhu@asc-csa.gc.ca*;
Tom.Lamarche@asc-csa.gc.ca; *Erick.Dupuis@asc-csa.gc.ca*)

** *Dept. of Aerospace Engineering, Ryerson University*
350 Victoria Street, Toronto, Ontario, Canada M5B 2K3
(E-mail: *gjliu@ryerson.ca*)

Abstract:
In this paper, a networked embedded control of modular robot manipulators without using joint torque sensing is presented. The proposed solution uses an effective control and communication mechanism based on the *virtual decomposition control* (VDC) approach with embedded FPGA (Field Programmable Gate Array) implementation. A hierarchical master-slaves control structure is used, supported by a high speed communication data bus. The master computer handles only kinematics computation and the dynamics-based computations are all performed by individual embedded FPGA module controllers. The *virtual stability* of each module is ensured, resulting in the L_2/L_∞ stability of the entire robot. Experimental results achieved on a three-module robot manipulator using harmonic drives are presented.

1. INTRODUCTION

Modular robotics has been extensively developed in the past two decades. Simply being formed with standardized modules, modular robot manipulators possess many advantages over conventional integrated robot manipulators in terms of re-reconfigurability, flexibility for structural change, and ease of replacement of faulty modules. Early development of modular robot manipulators can be traced back to the work by Schmitz et al. [1988], in which a CMU modular robot manipulator using a parallel-bus-like communication link clocked at 500 kHz was reported. Two years later, Fukuda and Kawauchi [1990] introduced the concept of cellular robotics. Paredis and Khosla [1993] developed a reconfigurable modular manipulator system (RMMS) with modular links and joints, in which kinematic configuration optimization was performed analytically for two DOF robots and numerically for multiple DOF robots. In the meantime, a (kinematic) configuration optimization procedure based on an assembly incidence matrix representation was presented by Chen and Burdick [1995]. Yim et al. [2000] developed a reconfigurable modular robot PolyBot targeting space applications. Hirzinger's group at DLR developed a light weight robot (LWR) with advanced mechanical modularity, see Hirzinger et al. [2001]. Shen et al. [2006] developed a SuperBot modular robot using an automatic docking mechanism. Recently, a modular robot manipulator using joint torque sensors was developed by Liu et al. [2008, 2011].

[1] This work was supported in part by the Natural Sciences and Engineering Research Council of Canada Discovery Grant 418295-2012.

However, the advantages of using modular robot manipulators do not come without a price. The naturally decentralized electro-mechanical structure of modular robot manipulators prevents many centralized control approaches (such as computed torque control) from being directly applied, leading to unsatisfied control performances, see Yim et al. [2007].

Efforts on improving control accuracy were indeed demonstrated in the past. To replace the robot dynamics computation needed by most inverse-model-based controllers, joint torque sensing approach was used instead, see Albu-Schaffer et al. [2007], Liu et al. [2008, 2011]. However, using joint torque sensing has its own drawbacks. A strain gauge is often sensitive to ambient temperature variations and is easily resulting in DC offset, see Hashimoto et al. [1993]. An optical torque sensor converts joint torque to joint deformation, see Hirose and Yoneda [1990], resulting in artificial joint flexibility that is undesirable for precision control. Furthermore, to achieve asymptotic tracking control, the joint torque measurements need to be directly fed back to compensate for the robot dynamics, see Liu et al. [2008]. While being tested very successfully in free motion such as in Liu et al. [2011], the direct use of joint torque measurement for robot dynamics compensation would necessarily create *algebraic loops* [2] about the joint torques for rigid-joint robots or about the (first or second order) time derivatives of the joint torques for flexible-joint robots, when asymptotic tracking control with rigid constrained tasks is concerned. Having *algebraic loops* makes robotic systems sensitive to unmodeled dynamics and disturbances and even results in instability when the

[2] See Section 2.10 in Zhu [2010].

gain of an *algebraic loop* reaches *one*. To avoid the *algebraic loop* issue, regulation tasks were reported in Albu-Schaffer et al. [2007].

The *virtual decomposition control* (VDC) approach provides a natural and effective solution to this long-standing thorny problem for the first time without using joint torque sensing, attributed to its naturally decentralized control structure, see Zhu et al. [1997], Zhu [2010], Zhu and Vukovich [2011], Zhu et al. [2013]. The VDC approach uses subsystem (such as links and joints of a complex robot) dynamics to conduct control design, while rigorously guaranteeing the stability and convergence of the entire complex robot. The unique feature of VDC in stability analysis is the definition of *virtual stability*. The stability of the entire complex robot is mathematically equivalent to the *virtual stability* of every subsystem. This fact allows us to convert a large complex problem to a few easy-to-solve simple problems with mathematical certainty, see Zhu [2010].

The contributions of this paper are summarized as follows: 1) A networked embedded control and communication system using VDC allows dynamics-based tracking control to be applied to modular robot manipulators without using joint torque sensing. 2) The master (host) computer handles only kinematics computation, while all dynamics-based control computations are fully handled by local embedded slave computers in a decentralized manner with guaranteed stability of the entire robot manipulator. 3) The implementation of module dynamics-based control on embedded FPGA devices enables much faster sampling rates, leading to a very high control precision.

This paper is organized as follows: the VDC based control and communications for modular robot manipulators are presented in Section 2 and the stability analysis is presented in Section 3. Finally, experimental results achieved on a three-module modular robot manipulator are reported in Section 4, followed by conclusion.

2. CONTROL AND COMMUNICATIONS

Assume that a complete modular robot manipulator comprises n modules, as illustrated in Fig. 1. Each module comprises two rigid links connected by a single-DOF joint, as illustrated in Fig. 2. At the end of each link lies a standard male or female electro-mechanical connection interface providing data and power connections to adjacent modules, see Zhu and Lamarche [2007] for details.

2.1 Communication System

The communication protocol is designed in such a way that the master node is able to broadcast information to all slave nodes and is able to extract information from any designated slave node, see Zhu and Lamarche [2007], Lamarche and Zhu [2007]. This protocol is a modified version of SpaceWire (IEEE 1355).

With respect to this communication protocol, two cycles with four actions are designed within each sampling period, see Fig. 3. The first communication cycle constitutes *Communications A* and *B*, and the second communication cycle constitutes *Communications C* and *D*.

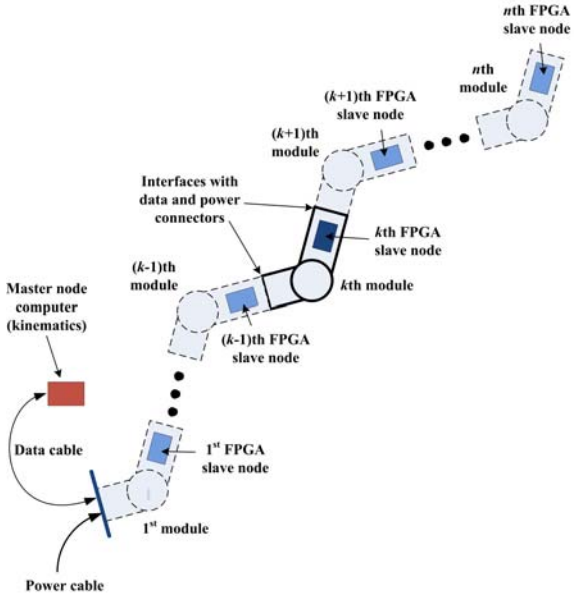

Fig. 1. A n-module modular robot manipulator.

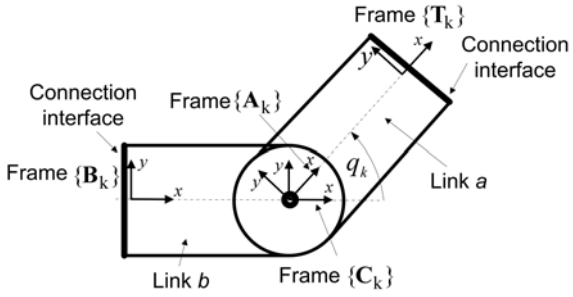

Fig. 2. Coordinate frames for the kth module.

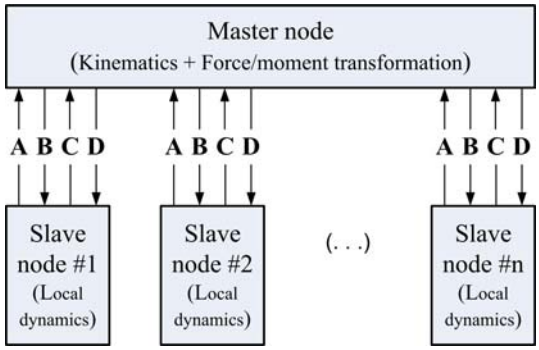

Fig. 3. Data exchange in communications.

2.2 Coordinate Frames

Four coordinate frames are attached to each module. For the kth module, $k \in \{1, n\}$, the four frames are illustrated in Fig. 2. Frames $\{\mathbf{A}_k\}$ and $\{\mathbf{C}_k\}$ share the same origin and are attached to Link a and Link b, respectively. The $\mathbf{z}$ axes of the two frames coincide with the joint axis. Frames $\{\mathbf{T}_k\}$ and $\{\mathbf{B}_k\}$ are attached to the two connection interfaces of the kth module, respectively, with their $\mathbf{x}$ axes aligning with the two link axes.

2.3 Communications and Control Computations

The entire communication and control computation process is summarized below.

Step 1: Perform *Communication A*: the master node extracts $q_k \in \mathbb{R}$ and $\dot{q}_k \in \mathbb{R}$ from the kth slave node for all $k \in \{1, n\}$, where q_k and $\dot{q}_k$ denote the joint position and velocity of the kth module.

Step 2: The master node computes the required joint velocity

$$\dot{q}_{kr} = \dot{q}_{kd} + \lambda(q_{kd} - q_k) \tag{1}$$

for all $k \in \{1, n\}$, where $q_{kd} \in \mathbb{R}$ denotes the desired joint position for joint k and $\lambda > 0$ is a control constant.

Then, the master node computes the linear/angular velocity vectors using

$$^{\mathbf{C}_k}V = {}^{\mathbf{B}_k}\mathbf{U}^T_{\mathbf{C}_k}\, {}^{\mathbf{B}_k}V \tag{2}$$

$$^{\mathbf{T}_k}V = {}^{\mathbf{C}_k}\mathbf{U}^T_{\mathbf{T}_k}\, {}^{\mathbf{C}_k}V + {}^{\mathbf{A}_k}\mathbf{U}^T_{\mathbf{T}_k}\mathbf{z}_\tau \dot{q}_k \tag{3}$$

$$^{\mathbf{B}_{(k+1)}}V = {}^{\mathbf{T}_k}\mathbf{U}^T_{\mathbf{B}_{(k+1)}}\, {}^{\mathbf{T}_k}V \tag{4}$$

with $\mathbf{z}_\tau = [0, 0, 0, 0, 0, 1]^T \in \mathbb{R}^6$, where ${}^{\alpha}V \in \mathbb{R}^6$, $\alpha \in \{\mathbf{A}_k, \mathbf{B}_k, \mathbf{C}_k, \mathbf{T}_k, \mathbf{B}_{k+1}\}$, denotes the linear/angular velocity vector of frame $\{\alpha\}$, expressed in frame $\{\alpha\}$, as defined by Definition 2.8 in [Zhu, 2010, page 29]; ${}^{\alpha}\mathbf{U}_{\beta} \in \mathbb{R}^{6\times 6}$ is a force/moment transformation matrix defined by (2.65) in Zhu [2010]. With ${}^{\mathbf{B}_1}V = 0$, Eqs. (2)-(4) are used recursively to obtain ${}^{\mathbf{C}_k}V \in \mathbb{R}^6$ for all $k \in \{1, n\}$.

Accordingly, the master node computes the required linear/angular velocity vectors using

$$^{\mathbf{C}_k}V_r = {}^{\mathbf{B}_k}\mathbf{U}^T_{\mathbf{C}_k}\, {}^{\mathbf{B}_k}V_r \tag{5}$$

$$^{\mathbf{T}_k}V_r = {}^{\mathbf{C}_k}\mathbf{U}^T_{\mathbf{T}_k}\, {}^{\mathbf{C}_k}V_r + {}^{\mathbf{A}_k}\mathbf{U}^T_{\mathbf{T}_k}\mathbf{z}_\tau \dot{q}_{kr} \tag{6}$$

$$^{\mathbf{B}_{(k+1)}}V_r = {}^{\mathbf{T}_k}\mathbf{U}^T_{\mathbf{B}_{(k+1)}}\, {}^{\mathbf{T}_k}V_r \tag{7}$$

where variables with subscript "r" refer to the corresponding required variables. With ${}^{\mathbf{B}_1}V_r = 0$, Eqs. (5)-(7) are used recursively to obtain ${}^{\mathbf{C}_k}V_r \in \mathbb{R}^6$ for all $k \in \{1, n\}$.

Step 3: Perform *Communication B*: the master node sends $\dot{q}_{kr} \in \mathbb{R}$, ${}^{\mathbf{C}_k}V \in \mathbb{R}^6$, ${}^{\mathbf{C}_k}V_r \in \mathbb{R}^6$, and ${}^{\mathbf{C}_k}\mathbf{R}_{\mathbf{I}}\mathbf{g} \in \mathbb{R}^3$ to the kth slave node for all $k \in \{1, n\}$, where ${}^{\mathbf{C}_k}\mathbf{R}_{\mathbf{I}} \in \mathbb{R}^{3\times 3}$ is a rotation matrix that transforms a three dimensional vector expressed in inertial frame $\{\mathbf{I}\}$ to the same vector expressed in frame $\{\mathbf{C}_k\}$ and $\mathbf{g} = [0, 0, 9.8]^T \in \mathbb{R}^3$ denotes the gravitational vector.

Step 4: The kth slave node computes

$$^{\mathbf{A}_k}V = {}^{\mathbf{C}_k}\mathbf{U}^T_{\mathbf{A}_k}\, {}^{\mathbf{C}_k}V + \mathbf{z}_\tau \dot{q}_k \tag{8}$$

$$^{\mathbf{A}_k}V_r = {}^{\mathbf{C}_k}\mathbf{U}^T_{\mathbf{A}_k}\, {}^{\mathbf{C}_k}V_r + \mathbf{z}_\tau \dot{q}_{kr} \tag{9}$$

after receiving $\dot{q}_{kr} \in \mathbb{R}$, ${}^{\mathbf{C}_k}V \in \mathbb{R}^6$, and ${}^{\mathbf{C}_k}V_r \in \mathbb{R}^6$ from the master node. Then, compute the required net force/moment vectors of the two rigid links using

$$^{\mathbf{A}_k}F^*_r = \mathbf{Y}_{\mathbf{A}_k}\hat{\theta}_{\mathbf{A}_k} + \mathbf{K}_{\mathbf{A}_k}\left({}^{\mathbf{A}_k}V_r - {}^{\mathbf{A}_k}V\right) \tag{10}$$

$$^{\mathbf{C}_k}F^*_r = \mathbf{Y}_{\mathbf{C}_k}\hat{\theta}_{\mathbf{C}_k} + \mathbf{K}_{\mathbf{C}_k}\left({}^{\mathbf{C}_k}V_r - {}^{\mathbf{C}_k}V\right) \tag{11}$$

where $\mathbf{K}_{\mathbf{A}_k} \in \mathbb{R}^{6\times 6}$ and $\mathbf{K}_{\mathbf{C}_k} \in \mathbb{R}^{6\times 6}$ are two positive-definite gain matrices characterizing velocity feedback control; $\mathbf{Y}_{\mathbf{A}_k}\hat{\theta}_{\mathbf{A}_k}$ and $\mathbf{Y}_{\mathbf{C}_k}\hat{\theta}_{\mathbf{C}_k}$ denote the model based feedforward compensation terms defined by

$$\mathbf{Y}_{\mathbf{A}_k}\theta_{\mathbf{A}_k} = \mathbf{M}_{\mathbf{A}_k}\frac{d}{dt}({}^{\mathbf{A}_k}V_r) + \mathbf{C}_{\mathbf{A}_k}({}^{\mathbf{A}_k}\omega)\,{}^{\mathbf{A}_k}V_r + \mathbf{G}_{\mathbf{A}_k} \tag{12}$$

$$\mathbf{Y}_{\mathbf{C}_k}\theta_{\mathbf{C}_k} = \mathbf{M}_{\mathbf{C}_k}\frac{d}{dt}({}^{\mathbf{C}_k}V_r) + \mathbf{C}_{\mathbf{C}_k}({}^{\mathbf{C}_k}\omega)\,{}^{\mathbf{C}_k}V_r + \mathbf{G}_{\mathbf{C}_k} \tag{13}$$

based on the physical link dynamics

$$\mathbf{M}_{\mathbf{A}_k}\frac{d}{dt}({}^{\mathbf{A}_k}V) + \mathbf{C}_{\mathbf{A}_k}({}^{\mathbf{A}_k}\omega)\,{}^{\mathbf{A}_k}V + \mathbf{G}_{\mathbf{A}_k} = {}^{\mathbf{A}_k}F^* \tag{14}$$

$$\mathbf{M}_{\mathbf{C}_k}\frac{d}{dt}({}^{\mathbf{C}_k}V) + \mathbf{C}_{\mathbf{C}_k}({}^{\mathbf{C}_k}\omega)\,{}^{\mathbf{C}_k}V + \mathbf{G}_{\mathbf{C}_k} = {}^{\mathbf{C}_k}F^* \tag{15}$$

where the detailed expressions of $\mathbf{M}_{\mathbf{A}_k}$, $\mathbf{M}_{\mathbf{C}_k}$, $\mathbf{C}_{\mathbf{A}_k}({}^{\mathbf{A}_k}\omega)$, $\mathbf{C}_{\mathbf{C}_k}({}^{\mathbf{C}_k}\omega)$, $\mathbf{G}_{\mathbf{A}_k}$, and $\mathbf{G}_{\mathbf{C}_k}$ were defined on page 31 of Zhu [2010].

The estimated parameter vectors $\hat{\theta}_{\mathbf{A}_k} \in \mathbb{R}^{13}$ and $\hat{\theta}_{\mathbf{C}_k} \in \mathbb{R}^{13}$ are to be updated. Define

$$\mathbf{s}_{\mathbf{A}_k} = \mathbf{Y}^T_{\mathbf{A}_k}\left({}^{\mathbf{A}_k}V_r - {}^{\mathbf{A}_k}V\right) \tag{16}$$

$$\mathbf{s}_{\mathbf{C}_k} = \mathbf{Y}^T_{\mathbf{C}_k}\left({}^{\mathbf{C}_k}V_r - {}^{\mathbf{C}_k}V\right). \tag{17}$$

The $\mathcal{P}$ function defined by Definition 2.11 in [Zhu, 2010, page 32] is used to update each element of $\hat{\theta}_{\mathbf{A}_k} \in \mathbb{R}^{13}$ and $\hat{\theta}_{\mathbf{C}_k} \in \mathbb{R}^{13}$ as

$$\hat{\theta}_{\mathbf{A}_k\gamma} = \mathcal{P}\left(s_{\mathbf{A}_k\gamma}, \rho_{\mathbf{A}_k\gamma}, \underline{\theta}_{\mathbf{A}_k\gamma}, \overline{\theta}_{\mathbf{A}_k\gamma}, t\right),\ \gamma \in \{1, 13\} \tag{18}$$

$$\hat{\theta}_{\mathbf{C}_k\gamma} = \mathcal{P}\left(s_{\mathbf{C}_k\gamma}, \rho_{\mathbf{C}_k\gamma}, \underline{\theta}_{\mathbf{C}_k\gamma}, \overline{\theta}_{\mathbf{C}_k\gamma}, t\right),\ \gamma \in \{1, 13\} \tag{19}$$

where $\hat{\theta}_{\mathbf{A}_k\gamma}$ denotes the γth element of $\hat{\theta}_{\mathbf{A}_k} \in \mathbb{R}^{13}$ and $\hat{\theta}_{\mathbf{C}_k\gamma}$ denotes the γth element of $\hat{\theta}_{\mathbf{C}_k} \in \mathbb{R}^{13}$; $s_{\mathbf{A}_k\gamma}$ denotes the γth element of $\mathbf{s}_{\mathbf{A}_k}$ defined by (16) and $s_{\mathbf{C}_k\gamma}$ denotes the γth element of $\mathbf{s}_{\mathbf{C}_k}$ defined by (17); $\rho_{\mathbf{A}_k\gamma} > 0$ and $\rho_{\mathbf{C}_k\gamma} > 0$ are update gains; $\underline{\theta}_{\mathbf{A}_k\gamma}$ and $\overline{\theta}_{\mathbf{A}_k\gamma}$ denote the lower and upper bounds of $\theta_{\mathbf{A}_k\gamma}$ - the γth element of $\theta_{\mathbf{A}_k} \in \mathbb{R}^{13}$; and $\underline{\theta}_{\mathbf{C}_k\gamma}$ and $\overline{\theta}_{\mathbf{C}_k\gamma}$ denote the lower and upper bounds of $\theta_{\mathbf{C}_k\gamma}$ - the γth element of $\theta_{\mathbf{C}_k} \in \mathbb{R}^{13}$.

The computations in this step are to be performed in a parallel manner.

Step 5: Perform *Communication C*: the master node extracts ${}^{\mathbf{A}_k}F^*_r \in \mathbb{R}^6$ and ${}^{\mathbf{C}_k}F^*_r \in \mathbb{R}^6$ from the kth slave node for all $k \in \{1, n\}$.

Step 6: The master node computes the required force/moment vectors using

$$^{\mathbf{A}_k}F_r = {}^{\mathbf{A}_k}F^*_r + {}^{\mathbf{A}_k}\mathbf{U}_{\mathbf{T}_k}\, {}^{\mathbf{T}_k}F_r \tag{20}$$

$$^{\mathbf{B}_k}F_r = {}^{\mathbf{B}_k}\mathbf{U}_{\mathbf{C}_k}\, {}^{\mathbf{C}_k}F^*_r + {}^{\mathbf{B}_k}\mathbf{U}_{\mathbf{A}_k}\, {}^{\mathbf{A}_k}F_r \tag{21}$$

$$^{\mathbf{T}_{(k-1)}}F_r = {}^{\mathbf{T}_{(k-1)}}\mathbf{U}_{\mathbf{B}_k}\, {}^{\mathbf{B}_k}F_r \tag{22}$$

from the robot tip toward the base with ${}^{\mathbf{T}_n}F_r = 0$. This computation is based on the physical force/moment transformation equations

$$ {}^{\mathbf{A}_k}F = {}^{\mathbf{A}_k}F^* + {}^{\mathbf{A}_k}\mathbf{U}_{\mathbf{T}_k}\,{}^{\mathbf{T}_k}F \tag{23} $$

$$ {}^{\mathbf{B}_k}F = {}^{\mathbf{B}_k}\mathbf{U}_{\mathbf{C}_k}\,{}^{\mathbf{C}_k}F^* + {}^{\mathbf{B}_k}\mathbf{U}_{\mathbf{A}_k}\,{}^{\mathbf{A}_k}F \tag{24} $$

$$ {}^{\mathbf{T}_{(k-1)}}F = {}^{\mathbf{T}_{(k-1)}}\mathbf{U}_{\mathbf{B}_k}\,{}^{\mathbf{B}_k}F \tag{25} $$

where ${}^{\alpha}F \in \mathbb{R}^6$, $\alpha \in \{\mathbf{A}_k, \mathbf{B}_k, \mathbf{C}_k, \mathbf{T}_k, \mathbf{T}_{k-1}\}$, denotes the force/moment vector of frame $\{\alpha\}$, expressed in frame $\{\alpha\}$, as defined by Definition 2.9 in [Zhu, 2010, page 29].

Step 7: Perform *Communication D*: the master node sends

$$ \tau_{ak} = \mathbf{z}_\tau^T\,{}^{\mathbf{A}_k}F_r \in \mathbb{R} \tag{26} $$

to the kth slave node for all $k \in \{1, n\}$.

Step 8: Given the joint dynamics of the kth slave node as

$$ I_{mk}\ddot{q}_k + f_k + d_k = \tau_k - \mathbf{z}_\tau^T\,{}^{\mathbf{A}_k}F \tag{27} $$

where I_{mk} is the joint moment of inertia, f_k is the joint friction, and d_k is a constant disturbance, the joint control torque τ_k is designed as

$$ \tau_k = \tau_k^* + \tau_{ak} \tag{28} $$

with

$$ \tau_k^* = \hat{I}_{mk}\ddot{q}_{kr} + f_{kr} + k_k(\dot{q}_{kr} - \dot{q}_k) + \hat{d}_k \tag{29} $$

and τ_{ak} from (26), where $k_k > 0$ is a control gain, $\hat{I}_{mk}$ and $\hat{d}_k$ denoting the estimates of I_{mk} and d_k, respectively, and f_{kr} is the friction compensation term for friction f_k subject to

$$ [f_{kr} - f_k][\dot{q}_{kr} - \dot{q}_k] \geq s_k(t) \tag{30} $$

with

$$ \int_0^\infty s_k(t)dt \geq -\gamma_0 \tag{31} $$

and $0 \leq \gamma_0 < \infty$.

The two parameter estimates $\hat{I}_{mk}$ and $\hat{d}_k$ are updated by using the $\mathcal{P}$ function (given by Definition 2.11 in [Zhu, 2010, page 32]) as

$$ \hat{I}_{mk} = \mathcal{P}\left(s_{mk}, \rho_{mk}, \underline{I}_{mk}, \overline{I}_{mk}, t\right) \tag{32} $$

$$ \hat{d}_k = \mathcal{P}\left(s_{dk}, \rho_{dk}, \underline{d}_k, \overline{d}_k, t\right) \tag{33} $$

with

$$ s_{mk} = (\dot{q}_{kr} - \dot{q}_k)\ddot{q}_{kr} \tag{34} $$

$$ s_{dk} = (\dot{q}_{kr} - \dot{q}_k) \tag{35} $$

where $\rho_{mk} > 0$ and $\rho_{dk} > 0$ are two update gains; $\underline{I}_{mk} > 0$ and $\overline{I}_{mk} > 0$ denote the lower and upper bounds of I_{mk}; and $\underline{d}_k$ and $\overline{d}_k$ denote the lower and upper bounds of d_k.

Remark 2.1: It can be easily proven that many friction compensation approaches satisfy condition (30). This category includes Coulomb friction compensation, viscous friction compensation, and even the LuGre model based friction compensation, see Zhu [2010a].

3. STABILITY ANALYSIS

A non-negative accompanying function

$$ \nu_{mk} = \nu_{\mathbf{A}_k} + \nu_{\mathbf{C}_k} + \nu_k \tag{36} $$

is assigned to the kth slave node, $k \in \{1, n\}$, where $\nu_{\mathbf{A}_k} \geq 0$ and $\nu_{\mathbf{C}_k} \geq 0$ are assigned to the two links, respectively, and $\nu_k \geq 0$ is assigned to the joint. The three non-negative functions have expressions as

$$ \begin{aligned} \nu_{\mathbf{A}_k} = {} & \frac{1}{2}\left({}^{\mathbf{A}_k}V_r - {}^{\mathbf{A}_k}V\right)^T \mathbf{M}_{\mathbf{A}_k}\left({}^{\mathbf{A}_k}V_r - {}^{\mathbf{A}_k}V\right) \\ & + \frac{1}{2}\sum_{\gamma=1}^{13}\left(\theta_{\mathbf{A}_k\gamma} - \hat{\theta}_{\mathbf{A}_k\gamma}\right)^2/\rho_{\mathbf{A}_k\gamma} \end{aligned} \tag{37} $$

$$ \begin{aligned} \nu_{C_k} = {} & \frac{1}{2}\left({}^{\mathbf{C}_k}V_r - {}^{\mathbf{C}_k}V\right)^T \mathbf{M}_{\mathbf{C}_k}\left({}^{\mathbf{C}_k}V_r - {}^{\mathbf{C}_k}V\right) \\ & + \frac{1}{2}\sum_{\gamma=1}^{13}\left(\theta_{\mathbf{C}_k\gamma} - \hat{\theta}_{\mathbf{C}_k\gamma}\right)^2/\rho_{\mathbf{C}_k\gamma} \end{aligned} \tag{38} $$

$$ \begin{aligned} \nu_k = {} & \frac{1}{2}I_{mk}\left(\dot{q}_{kr} - \dot{q}_k\right)^2 + \frac{1}{2}(I_{mk} - \hat{I}_{mk})^2/\rho_{mk} \\ & + \frac{1}{2}(d_k - \hat{d}_k)^2/\rho_{dk}. \end{aligned} \tag{39} $$

Doing mathematical operations using (2)-(35) and Lemma 2.9 in Zhu [2010] leads to

$$ \begin{aligned} \dot{\nu}_{mk} = {} & \dot{\nu}_{\mathbf{A}_k} + \dot{\nu}_{\mathbf{C}_k} + \dot{\nu}_k \\ \leq {} & -\left({}^{\mathbf{A}_k}V_r - {}^{\mathbf{A}_k}V\right)^T \mathbf{K}_{\mathbf{A}_k}\left({}^{\mathbf{A}_k}V_r - {}^{\mathbf{A}_k}V\right) \\ & -\left({}^{\mathbf{C}_k}V_r - {}^{\mathbf{C}_k}V\right)^T \mathbf{K}_{\mathbf{C}_k}\left({}^{\mathbf{C}_k}V_r - {}^{\mathbf{C}_k}V\right) \\ & -k_k(\dot{q}_{kr} - \dot{q}_k)^2 - s_k(t) + p_{\mathbf{B}_k} - p_{\mathbf{T}_k} \end{aligned} \tag{40} $$

where $s_k(t)$ is subject to (31) and $p_{\mathbf{B}_k}$ and $p_{\mathbf{T}_k}$ represent the *virtual power flows* defined by

$$ p_{\mathbf{B}_k} = ({}^{\mathbf{B}_k}V_r - {}^{\mathbf{B}_k}V)^T({}^{\mathbf{B}_k}F_r - {}^{\mathbf{B}_k}F) \tag{41} $$

$$ p_{\mathbf{T}_k} = ({}^{\mathbf{T}_k}V_r - {}^{\mathbf{T}_k}V)^T({}^{\mathbf{T}_k}F_r - {}^{\mathbf{T}_k}F) \tag{42} $$

at the two interfaces of the kth module.

The two terms $p_{\mathbf{B}_k}$ and $-p_{\mathbf{T}_k}$ appearing in the right hand side of (40) are named *virtual power flows* (by Definition 2.16 in Zhu [2010]) at the two interfaces of the kth module. They behave as a positive (plus sign) and a negative (minus sign) "stability connectors" of the kth module to the remaining modules. Having *virtual power flows* is a unique characteristic of the definition of *virtual stability* in Zhu [2010]. If every module (when being combined with its respective control equations) is *virtually stable*, then Theorem 2.1 in Zhu [2010] ensures that the complete robot (system) is stable. This is because all the *virtual power flows* of the entire system cancel out with each other as if each positive "stability connector" is connected to its corresponding negative "stability connector." In fact, using (4) and (7) results in

$$ p_{\mathbf{T}_k} = p_{\mathbf{B}_{(k+1)}},\ k \in \{1, n-1\} \tag{43} $$

which implies

$$ \sum_{k=1}^{n}\left(p_{B_k} - p_{T_k}\right) = 0 \tag{44} $$

for given $p_{\mathbf{B}_1} = 0$ (with zero velocity) and $p_{\mathbf{T}_n} = 0$ (with zero force) of a n-module modular robot manipulator.

Thus, the non-negative function for the entire robot is chosen as

$$\nu = \sum_{k=1}^{n} \nu_{mk}. \tag{45}$$

It follows from (36), (40), and (44) that

$$\begin{aligned}\dot{\nu} \leq & -\sum_{k=1}^{n} \left({}^{\mathbf{A}_k}V_r - {}^{\mathbf{A}_k}V\right)^T \mathbf{K}_{\mathbf{A}_k} \left({}^{\mathbf{A}_k}V_r - {}^{\mathbf{A}_k}V\right) \\ & -\sum_{k=1}^{n} \left({}^{\mathbf{C}_k}V_r - {}^{\mathbf{C}_k}V\right)^T \mathbf{K}_{\mathbf{C}_k} \left({}^{\mathbf{C}_k}V_r - {}^{\mathbf{C}_k}V\right) \\ & -\sum_{k=1}^{n} k_k(\dot{q}_{kr} - \dot{q}_k)^2 - \sum_{k=1}^{n} s_k(t). \end{aligned} \tag{46}$$

In view of (36), (45), and (46), it follows from Lemma 2.3 and Lemma 2.4 in Zhu [2010] that

$$\dot{q}_{kr} - \dot{q}_k \in L_2 \cap L_\infty, \quad \forall k \in \{1, n\} \tag{47}$$

holds, leading to

$$q_{kd} - q_k \in L_2 \cap L_\infty, \quad \forall k \in \{1, n\} \tag{48}$$

$$\dot{q}_{kd} - \dot{q}_k \in L_2 \cap L_\infty, \quad \forall k \in \{1, n\} \tag{49}$$

from (1).

The asymptotic stability in the sense of

$$q_{kd} - q_k \to 0 \tag{50}$$

$$\dot{q}_{kd} - \dot{q}_k \to 0 \tag{51}$$

for $\forall k \in \{1, n\}$ follows immediately from using bounded reference signals, leading to bounded control τ_k and bounded joint acceleration $\ddot{q}_k$, $k \in \{1, n\}$, in view of Tao [1997].

4. EXPERIMENT

A three-module modular robot manipulator presented in Zhu et al. [2013] is used to test the control algorithm.

The master node is a PowerPC 405 clocked at 300 MHz, computing the kinematics of the robot including (1), (2)-(7), and (20)-(22), with a sampling frequency of 1000 Hz.

A Virtex II-1000 FPGA logic device clocked at 50 MHz is used as a slave node computing (8)-(11), (16)-(19), (28), (29), and (32)-(35). In computing (29), (1) is used again and updated at 50 MHz.

The desired trajectories of the three joints are designed as

$$\begin{aligned} q_{1d}(t) &= q_d(t) \\ q_{2d}(t) &= 2q_d(t) \\ q_{3d}(t) &= 3q_d(t) \end{aligned}$$

with

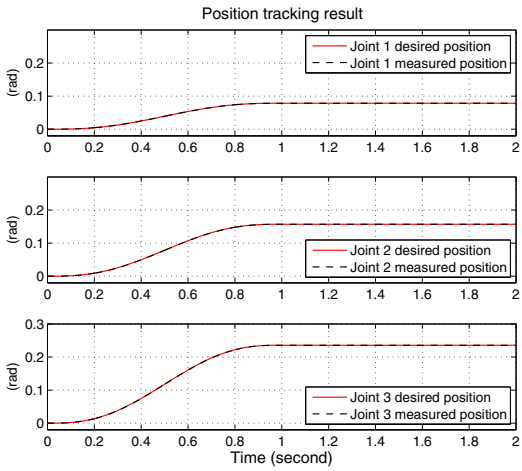

Fig. 4. Position tracking result of a 3-module robot.

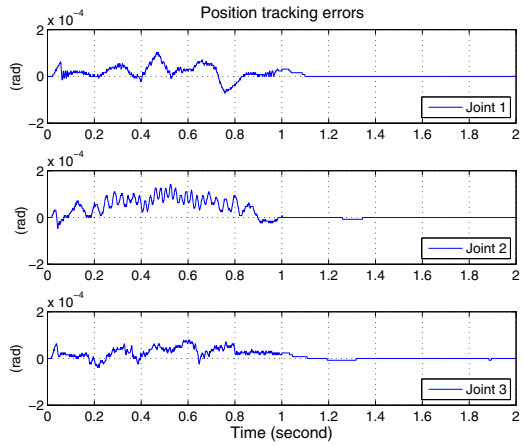

Fig. 5. Position tracking errors.

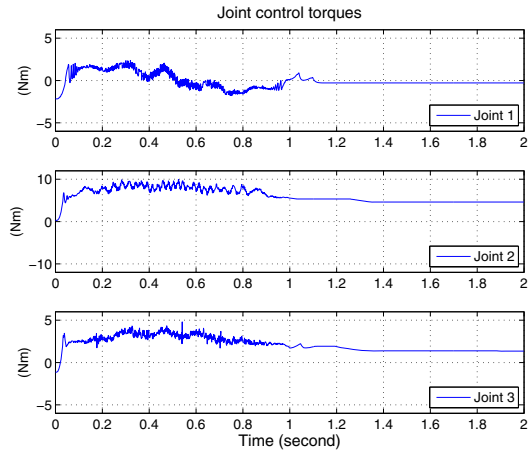

Fig. 6. Joint control torques.

$$\begin{aligned} q_d(t) = & 6(p_f - p_0)\,(t/t_f)^5 - 15(p_f - p_0)\,(t/t_f)^4 \\ & +10(p_f - p_0)\,(t/t_f)^3 + p_0 \end{aligned}$$

where $p_0 = 0$ (rad), $p_f = 0.0785$ (rad), and $t_f = 1$ (second) denote the initial position, the final position, and the trajectory duration, respectively.

The position tracking result is illustrated in Fig. 4 with the position tracking errors and the joint control torques being illustrated in Figs. 5 and 6, respectively. The maximum position tracking errors are limited by 0.0001 (rad).

The detailed description about the experiments can be found in Zhu et al. [2013].

5. CONCLUSION

A networked embedded control approach has been developed in this paper to solve a long standing problem, the lack of control precision, associated with modular robot manipulators. The developed control framework uses *virtual decomposition control* (VDC) approach without needing joint torque sensing. The decentralized control structure of VDC fits naturally with the decentralized electro-mechanical structure of the modular robot manipulators. The master computer handles all kinematics computations and initiates communications, while leaving all dynamics-based control computations to individually embedded slave controllers. The validity of the developed control approach has been ensured by both stability proof and experimental verification.

REFERENCES

Albu-Schaffer, A., Ott, C., and Hirzinger, G. (2007). A unified passivity-based control framework for position, torque, and impedance control of flexible joint robots. *Int. J. robotics Research*, 26(1):23–39.

Chen, I. M. and Burdick, J. W. (1995). Determining task optimal modular robot assembly configurations. *Proc. of 1995 IEEE Int. Conf. Robotics and Automation*, 132–137.

Fukuda, T. and Kawauchi, Y. (1990). Cellular robotic system (CEBOT) as one of the realization of self-organizing intelligent universal manipulator. *Proc. of 1990 IEEE Int. Conf. Robotics and Automation*, 662–667.

Hashimoto, M., Kiyosawa, Y., and Paul, R. P. (1993). A torque sensing technique for robots with harmonic drives. *IEEE Trans. Robotics and Automation*, 9(1):108–116.

Hirose, S. and Yoneda, K. (1990). Development of optical 6-axial force sensor and its signal calibration considering non-linear interference. *Proc. of 1990 IEEE Int. Conf. Robotics and Automation*, 46–53, Cincinnati, OH.

Hirzinger, G., Albu-Schaffer, A., Hahnle, M., Schaefer, I., and Sporer, N. (2001). On a new generation of torque controlled light-weight robots. *Proc. of 2001 IEEE Int. Conf. Robotics and Automation*, 3356–3363, Seoul, Korea.

Lamarche, T. and Zhu, W.-H. (2007). A virtual decomposition control based communication network for modular robots applications. *First International Workshop on Networking Technology for Robotics and Applications (NeTRA 2007) in conjunction with ICCCN 2007*, 1321–1326, Honolulu, Hawaii.

Liu, G., Abdul, S., and Goldenberg, A. A. (2008). Distributed control of modular and reconfigurable robot with torque sensing. *Robotica*, 26(1):75–84.

Liu, G., Liu, Y., and Goldenberg, A. A. (2011). Design, analysis, and control of a spring-assisted modular and reconfigurable robot. *IEEE/ASME Trans. Mechatronics*, 16(4):695–706.

Paredis, C. J. J. and Khosla, P. K. (1993). Kinematic design of serial link manipulators from task specifications. *Int. J. Robotics Research*, 12(3):274–287.

Schmitz, D., Khosla, P., and Kanade, T. (1988). The CMU reconfigurable modular manipulator system. Institute for Software Research, Carnegie Mellon University.

Shen, W.-M., Krivokon, M., Chiu, H., Everist, J., Rubenstein, M., and Venkatesh, J. (2006). Multimode locomotion via SuperBot reconfigurable robots. *Autonomous Robots*, 20(2):165–177.

Tao, G. (1997). A simple alternative to the Barbălat lemma. *IEEE Trans. Automatic Control*, 42(5):698.

Yim, M., Duff, D. G., and Roufas, K. D. (2000). Polybot: a modular reconfigurable robot. *Proc. of 2000 IEEE Int. Conf. Robotics and Automation*, 514–520, San Francisco, CA.

Yim, M., Shen, W.-M., Salemi, B., Rus, D., Moll, M., Lipson, H., Klavins, E., and Chirikjian, G. (2007). Modular self-reconfigurable robot systems. *IEEE Robotics and Automation Magazine*, 43–52.

Zhu, W.-H., Xi, Y.-G., Zhang, Z.-J., Bien, Z., and De Schutter, J. (1997). Virtual decomposition based control for generalized high dimensional robotic systems with complicated structure. *IEEE Trans. Robotics and Automation*, 13(3):411–436.

Zhu, W.-H. and Lamarche, T. (2007). Modular robot manipulators based on virtual decomposition control. *Proc. of 2007 IEEE Int. Conf. Robotics and Automation*, 2235–2240, Rome, Italy.

Zhu, W.-H. (2010). *Virtual Decomposition Control*, STAR Series No. 60, Springer-Verlag, 2010.

Zhu, W.-H. (2010a). FPGA-based adaptive friction compensation for precision control of harmonic drives. *Proc. of 2010 IEEE Int. Conf. Robotics and Automation*, 4657–4662, Anchorage, Alaska.

Zhu, W.-H. and Vukovich, G. (2011). Virtual decomposition control for modular robot manipulator. *Preprint of 18th IFAC World Congress*, 13486–13491, Milan, Italy.

Zhu, W.-H., Lamarche, T., Dupuis, E., Jameux, D., Barnard, P., and Liu G. (2013). Precision control of modular robot manipulators: the VDC approach with embedded FPGA. *IEEE Trans. Robotics*, 29(5):1162–1179.